Schwarps: Locally Projective Image Warps Based on 2D Schwarzian Derivatives

Rahat Khan, Daniel Pizarro, and Adrien Bartoli

ISIT, UMR 6284 CNRS-UdA, Clermont-Ferrand, France

Abstract. Image warps -or just warps- capture the geometric deformation existing between two images of a deforming surface. The current approach to enforce a warp's smoothness is to penalize its second order partial derivatives. Because this favors locally affine warps, this fails to capture the local projective component of the image deformation. This may have a negative impact on applications such as image registration and deformable 3D reconstruction. We propose a novel penalty designed to smooth the warp while capturing the deformation's local projective structure. Our penalty is based on equivalents to the Schwarzian derivatives, which are projective differential invariants exactly preserved by homographies. We propose a methodology to derive a set of Partial Differential Equations with homographies as solutions. We call this system the Schwarzian equations and we explicitly derive them for 2D functions using differential properties of homographies. We name as Schwarp a warp which is estimated by penalizing the residual of Schwarzian equations. Experimental evaluation shows that Schwarps outperform existing warps in modeling and extrapolation power, and lead to far better results in Shape-from-Template and camera calibration from a deformable surface.

Keywords: Schwarzian Penalizer, Bending Energy, Projective Differential Invariants, Image Warps.

1 Introduction

Projective geometry studies the geometric properties of projective transformations. During the last 30 years, projective geometry has successfully modeled important problems in computer vision, such as image stitching [28], image registration [29] and Structure-from-Motion (SfM) [10,9]. These problems assume the scene is rigid. However, if the scene geometry deforms over time, the current tools from projective geometry cannot model it. They are thus insufficient for problems like Non-Rigid Structure-from-Motion (NRSfM) [30], Shape-from-Template[1] (SfT) [25] and non-rigid image registration [3]. In a deformable environment, a fundamental problem is the modeling of the image warp -or just warp-, the function which maps points between images of a deforming surface. A

[1] In SfT, the 3D shape of a deformable surface is computed from the warp between a template and an input image. The shape of the template is known a priori.

D. Fleet et al. (Eds.): ECCV 2014, Part IV, LNCS 8692, pp. 1–15, 2014.

warp is generally represented by a linear basis expansion such as the Thin-Plate Spline (TPS) [6], the tensor-product B-Spline (BS) [24], finite elements [23] and finite differences (as in optical flow) [11]. A warp is also generally assumed to be smooth or piecewise smooth. This is modeled by existing approaches as a penalty on the warp's derivatives. For instance, penalizing second order derivatives leads to the popular bending energy, which forces the warp to be locally affine. A direct consequence is that the local projective information cannot be captured by the warp. Interestingly, it was attempted to solve that problem by modeling the warp with rational basis expansion. This led to the Generalized TPS [5] and the NURBS warp [7]. Theoretically, rational warps can be smooth and capture the local projective structure. However, their main problem is that they are non-convex and may be unstable due to their rational structure. We propose a novel penalty which is able to smooth a warp while allowing it to capture the local projective structure. This penalty may be used to estimate *any* type of warp model. Therefore, it may be applied to linear basis expansions, and does not require the use of a rational warp. Our penalty is based on the theory of Projective Differential Geometry (PDG), which we argue is a fundamental tool in warp modeling. PDG is a branch of mathematics that studies the properties of projective transformations at an infinitesimal scale. So far, PDG has been used to a much smaller extent than projective geometry in computer vision [13,26]. An important result of PDG is the Schwarzian derivative [22]. It originated from the study of projective differential invariants, but also appears in many other fields of mathematics such as the dynamical system theory and differential equation solving. The Schwarzian derivative models cross-ratio at a differential level [22]. The cross-ratio of points is well-known in computer vision [17,14] as it represents a projective invariant between two images related by a homography. In $\mathbb{RP}_1$, cross-ratio is defined for 4 colinear points. In the differential cross-ratio the distances among these points are infinitesimal. The Schwarzian derivative is a differential operator that vanishes for functions that preserve the differential cross-ratio. The Schwarzian derivative is well defined in the 1D case [22,27]. However, we are interested in images and thus in the 2D case. Several extensions of the Schwarzian derivative to higher dimensions were proposed [15,19,21]. Computing Schwarzian derivatives of an image warp requires one to find a system of PDEs that, as in the case of the 1D Schwarzian derivative, has homographies as solutions. Unfortunately, it is far from straightforward to arrive from the existing multidimensional Schwarzians to the sought system of PDEs (see section 2.3 for details).

We bring two core contributions. The first one is a new derivation framework for the 1D Schwarzian derivative which extends to higher dimensions. In particular, we use our framework to explicitly derive a system of PDEs that we call the *2D Schwarzian equations*. Our second core contribution is the *Schwarp*, which is defined as an image warp which was estimated while penalizing our 2D Schwarzian equations, preserving local projective properties. The intuition underlying this penalizer is that a warp with small residuals for our 2D Schwarzian equations behaves locally like a homography. A Schwarp may be constructed

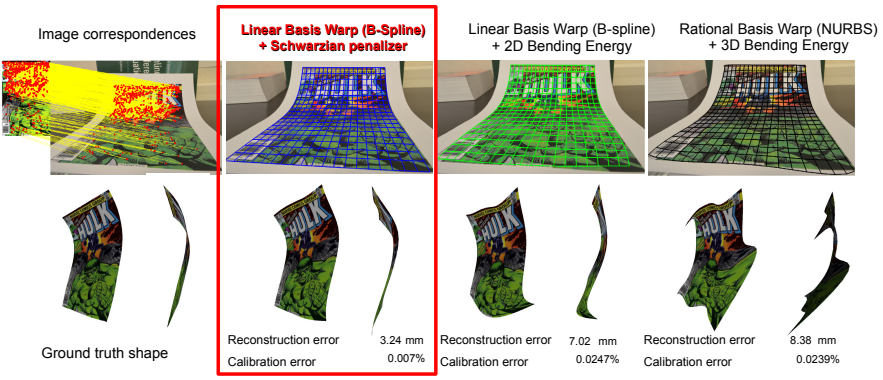

Fig. 1. Shape-from-Template (SfT) results for different warp models. The first column shows the input feature correspondences and the ground truth shape obtained by Structure-from-Motion for multiple images. In these examples, the BS-warp is used as the linear basis warp and the NURBS-warp as the rational basis warp. It is clear that the warp that uses Schwarzian equations as a penalizer improves accuracy over the other warps. SfT depends on the first derivative of the warp which is captured with our penalizer to a better extent.

with any warp representation and improves over classical approaches based on using the bending energy as a penalizer, favoring a locally affine behavior (see figure 1).

We report an extensive set of experimental results. Schwarps do better in two ways: *(i)* the warp's extrapolation power increases, especially in perspective imaging conditions, *(ii)* the accuracy of the warp's derivatives is improved by a large margin. We validated the impact of Schwarps on two applications: SfT [2] and camera calibration from a deformable surface [4].

2 Background on Projective Differential Invariants

Projective differential invariants have been studied in computer vision in a few previous papers [13,1]. In [13], the authors focus on qualitative local projective differential invariants whereas [1] focuses on non-algebraic planar curves. We now present one of the most fundamental projective differential invariants, the Schwarzian derivative which has rarely been studied in computer vision. We start our discussion with the cross-ratio of 4 points in the projective line and 5 points in the projective plane. We then give the differential version of the cross-ratio in the projective line, leading to the 1D Schwarzian derivative.

2.1 The Cross-Ratio

We consider 4 points t_1, t_2, t_3, t_4 in the projective line $\mathbb{RP}_1$. The cross-ratio on $\mathbb{RP}_1$ is defined by the following scalar $\Phi(t_1, t_2, t_3, t_4) = \frac{(t_1-t_3)(t_2-t_4)}{(t_2-t_3)(t_1-t_4)}$. Homographic transformations $\gamma : \mathbb{RP}_1 \to \mathbb{RP}_1$ preserve the cross-ratio:

$$\Phi(t_1, t_2, t_3, t_4) = \Phi(\gamma(t_1), \gamma(t_2), \gamma(t_3), \gamma(t_4)). \tag{1}$$

This directly extends to 4 colinear points in the projective plane $\mathbb{RP}_2$. For 5 non-colinear points in $\mathbb{RP}_2$, one may select one point as a reference and compute 4 direction vectors with the remaining 4 points. Replacing distances by inter-direction angles one obtains 2 different cross-ratios, representing 2 fundamental invariants of 5 points in the projective plane.

2.2 The 1D Schwarzian Derivative

The most popular projective differential invariant is the Schwarzian derivative [22]. We give its derivation as can be found in the literature. We consider a diffeomorphism γ which acts on 4 points $t_1, t_2, t_3, t_4 \in \mathbb{RP}_1$. We assume that the 4 points are spread so that t_2, t_3, t_4 can be defined by their distances to t_1 as a function of $\epsilon \in \mathbb{R}$: $t_2 = t_1 + \epsilon$, $t_3 = t_1 + 2\epsilon$ and $t_4 = t_1 + 3\epsilon$. So, the 4 points become $t_1, t_1 + \epsilon, t_1 + 2\epsilon, t_1 + 3\epsilon$ and they are related by the variable ϵ. The Schwarzian derivative measures the effect of γ on the cross-ratio as ϵ tends to zero. In other words, the Schwarzian derivative measures the cross-ratio of the points when they are infinitesimally close. To obtain the Schwarzian derivative one forms the Taylor expansion of Φ when ϵ goes to zero and keeps the first non-zero term of the expansion:

$$\Phi(\gamma(t_1), \gamma(t_2), \gamma(t_3), \gamma(t_4)) = \Phi(t_1, t_2, t_3, t_4) - \epsilon^2 S[\gamma](t_1) + O(\epsilon^3) \tag{2}$$

In the above equation $S[\gamma]$ is the Schwarzian derivative for $\mathbb{RP}_1$, defined by:

$$S[\gamma] = \frac{\gamma'''}{\gamma'} - \frac{3}{2}\left(\frac{\gamma''}{\gamma'}\right)^2 \tag{3}$$

The Schwarzian derivative $S[\gamma]$ has some remarkable properties. From equation (2) it is easy to see that if γ is a homography, $S[\gamma] = 0$ as the cross ratio is zero. Conversely, it can be proved that $S[\gamma] = 0$ implies that γ is a homography [21]. Therefore, homographies are the only solutions of the differential equation $S[\gamma] = 0$. With the Schwarzian derivative one can thus measure how close γ is to a homography. Unfortunately, this derivation of the Schwarzian derivative in $\mathbb{RP}_1$ does not readily extend to $\mathbb{RP}_2$.

2.3 Multidimensional Schwarzian Derivatives (MSDs)

The original Schwarzian derivative was only defined in 1D [12,8]. However, over the last few decades, mathematicians have extended it to higher dimensions. Ovsienko et al. [22] summarize a general two-step recipe to obtain MSDs for any group of diffeomorphisms:

1. Choose a group of diffeomorphisms and a subgroup G that has a 'nice' geometrical meaning (for instance, the projective group).
2. Find a G-invariant 1-cocycle on the group of diffeomorphisms.

Examples of MSDs can be found for different groups of diffeomorphisms. Oda [18] first defined an MSD for locally biholomorphic mappings. [19] proposed the conformal MSD whereas [20] proposed the 'Lagrangian Schwarzian' modeled on the group of symmetric matrices. The case of MSD for differential projective structures, which is the extension to higher dimensions of the 1D Schwarzian, has also been studied by several authors [15,16,21]. They provide as a general result for MSDs the 1-cocycle, that is a non-linear differential operator that vanishes for homographies. The 1-cocycle includes second order partial derivatives and rational terms. The 1-cocycle cannot be used to define the Schwarp as it also can vanish for other functions rather than homographies.

3 Schwarzian Equations in Two Dimensions

We propose to derive the Schwarzian equations, that is, a system of PDEs with homographies as solutions. Unlike MSDs that are described by the 1-cocycle, we define the multidimensional Schwarzian equations as a set of PDEs where each member of the set vanishes for homographies. Interestingly, our Schwarzian equations in 2D are quadratic second order PDEs. This allows us to optimize the Schwarp without using rational terms. We first show how to find the 1D Schwarzian derivative (3). We then use the same methodology to find the 2D Schwarzian equations.

3.1 The 1D Schwarzian Derivative

We define γ as a general projective function, formed by the ratio of two linear functions:

$$\gamma = \frac{\delta}{\zeta}, \qquad \text{where} \quad \delta'' = 0, \quad \zeta'' = 0 \quad \text{and} \quad \zeta \neq 0. \tag{4}$$

By multiplying equation (4) with ζ and taking its third order derivatives we obtain the following PDE:

$$\gamma'''\zeta + 3\gamma''\zeta' = 0. \tag{5}$$

Differentiating equation (4) and multiplying by ζ^2 on both sides we obtain:

$$\gamma'\zeta^2 = \delta'\zeta - \delta\zeta'. \tag{6}$$

By differentiating equation (6) we obtain:

$$\begin{aligned} \gamma''\zeta^2 + 2\gamma'\zeta\zeta' &= 0 \\ \zeta' &= -\frac{1}{2}\frac{\gamma''}{\gamma'}\zeta. \end{aligned} \tag{7}$$

We substitute equation (7) in equation (5), and cancel ζ and ζ'

$$\gamma''' - \frac{3}{2}\frac{(\gamma'')^2}{\gamma'} = 0. \tag{8}$$

Dividing equation (8) by γ' gives the 1D Schwarzian derivative as can be verified by directly comparing it to equation (3). Multiplying equation (8) by γ', we arrive at the following third order quadratic PDE:

$$\gamma'\gamma''' - \frac{3}{2}(\gamma'')^2 = 0. \tag{9}$$

The main difference between equation (9) and the Schwarzian derivative is that equation (9) does not have the rational term. Despite that, both of them, have only homographies as solution.

3.2 2D Schwarzian Equations

We propose a system of PDEs that represent the 2D Schwarzian equations. This system has by construction homographies as solutions

We define function $\eta : (u, v)^\top \to (x, y)^\top$ as an homography:

$$\eta = \begin{pmatrix}\eta^x & \eta^y\end{pmatrix}^\top \qquad \text{with} \qquad \eta^x = \frac{\delta^x}{\zeta} \quad \eta^y = \frac{\delta^y}{\zeta} \quad \zeta \neq 0, \tag{10}$$

and where δ^x, δ^y and ζ are linear scalar functions whose second order partial derivatives vanish:

$$\delta^x_{uu} = \zeta_{uu} = \delta^y_{uu} = 0 \quad \delta^x_{vv} = \zeta_{vv} = \delta^y_{vv} = 0 \quad \delta^x_{uv} = \zeta_{uv} = \delta^y_{uv} = 0. \tag{11}$$

We first multiply η^x and η^y by ζ and differentiate them with respect to u:

$$\eta^x_u\zeta + \eta^x\zeta_u = \gamma_u \qquad \eta^y_u\zeta + \eta^y\zeta_u = \delta_u. \tag{12}$$

We differentiate them again with respect to u using equations (11) to remove second order derivatives of δ^x, δ^y and ζ:

$$\eta^x_{uu}\zeta + 2\eta^x_u\zeta_u = 0 \qquad \eta^y_{uu}\zeta + 2\eta^y_u\zeta_u = 0. \tag{13}$$

By solving for ζ_u in equation (13), we find the first 2D Schwarzian equation:

$$\frac{\eta^x_{uu}\zeta}{2\eta^x_u} = \frac{\eta^y_{uu}\zeta}{2\eta^y_u} \tag{14}$$

$$\boxed{\eta^x_{uu}\eta^y_u - \eta^y_{uu}\eta^x_u = 0.} \tag{15}$$

We now multiply η^x and η^y by ζ and we differentiate twice with respect to v:

$$\eta^x_{vv}\zeta + 2\eta^x_v\zeta_v = 0 \qquad \eta^y_{vv}\zeta + 2\eta^y_v\zeta_v = 0. \tag{16}$$

Solving for ζ_v in equation (16) gives the second 2D Schwarzian equation:

$$\boxed{\eta^x_{vv}\eta^y_v - \eta^y_{vv}\eta^x_v = 0.} \tag{17}$$

We then take the partial derivatives of equations (12) with respect to v:

$$\eta^x_{uv}\zeta + \eta^x_u\zeta_v + \eta^x_v\zeta_u = 0 \qquad \eta^y_{uv}\zeta + \eta^y_u\zeta_v + \eta^y_v\zeta_u = 0. \tag{18}$$

Solving for ζ_v in equation (18) yields:

$$(\eta^x_{uv}\eta^y_u - \eta^y_{uv}\eta^x_u)\zeta + (\eta^x_v\eta^y_u - \eta^y_v\eta^x_u)\zeta_u = 0. \tag{19}$$

Multiplying the two equations in equation (13) by η^y_v and η^x_v respectively and subtracting them we obtain the following equation:

$$(\eta^x_{uu}\eta^y_v - \eta^y_{uu}\eta^x_v)\zeta - 2(\eta^x_v\eta^y_u - \eta^y_v\eta^x_u)\zeta_u = 0, \tag{20}$$

which we combine with equation (19) to remove ζ_u, giving the third 2D Schwarzian equation:

$$\boxed{(\eta^x_{uu}\eta^y_v - \eta^y_{uu}\eta^x_v) + 2(\eta^x_{uv}\eta^y_u - \eta^y_{uv}\eta^x_u) = 0.} \tag{21}$$

In a similar way we can obtain the fourth and last 2D Schwarzian equations by solving for ζ_v in equation (18) and combining the result with equation (16). The complete system of 4 2D Schwarzian equations is finally given by:

$$\text{2D-Schwarzian equations} \quad \begin{cases} S_1[\eta] = \eta^x_{uu}\eta^y_u - \eta^y_{uu}\eta^x_u = 0 \\ S_2[\eta] = \eta^x_{vv}\eta^y_v - \eta^y_{vv}\eta^x_v = 0 \\ S_3[\eta] = (\eta^x_{uu}\eta^y_v - \eta^y_{uu}\eta^x_v) + 2(\eta^x_{uv}\eta^y_u - \eta^y_{uv}\eta^x_u) = 0 \\ S_4[\eta] = (\eta^x_{vv}\eta^y_u - \eta^y_{vv}\eta^x_u) + 2(\eta^x_{uv}\eta^y_v - \eta^y_{uv}\eta^x_v) = 0. \end{cases} \tag{22}$$

In contrast with the third order 1D Schwarzian derivative, the 2D Schwarzian equations form a second order quadratic system of PDEs.

4 Modeling the Projection of Deforming Surfaces

The warp between two images of a plane is a homography. In that case, the 2D Schwarzian derivatives vanish, by definition. With a non-planar and possibly deforming surface, the image warp does not anymore satisfy the Schwarzian equations exactly. For a smooth surface deformation however, each small patch on the surface can be approximated by its tangent plane (see figure 2). The warp η can then be locally approximated by a homography between the projections of the tangent planes. The Schwarzian derivatives form differential invariants and we thus expect the system in equation (22) to have small residuals for the projection of infinitesimal planes.

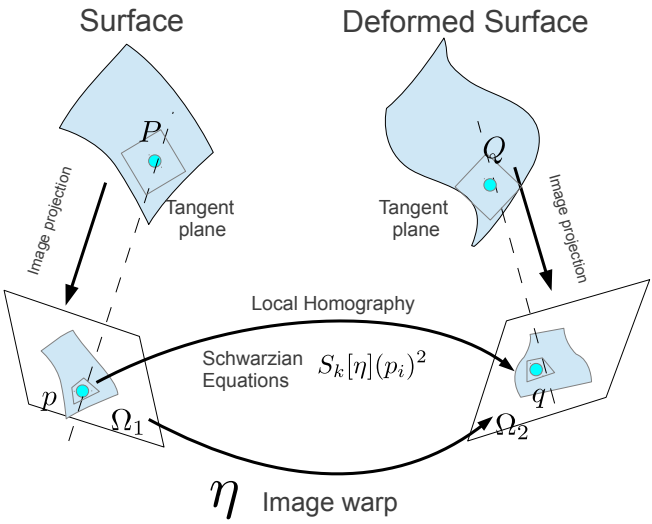

Fig. 2. The 2D Schwarzian derivatives have small residuals for the warp η between the images of a smooth deforming surface

4.1 The Schwarp

For an image warp $\eta : \Omega_1 \rightarrow \Omega_2$, the 2D Schwarzian derivatives measure how near is η from a homography infinitesimally at each point. We define the Schwarp as a warp whose 2D Schwarzian derivatives were penalized for its estimation. As a result the Schwarp can be smooth while preserving differential projective properties.

The Schwarp is defined as the solution of the following variational problem:

$$\min_{\eta} \epsilon_d[\eta] + \epsilon_s[\eta], \tag{23}$$

where $\epsilon_d[\eta]$ is a data term measuring registration error (for instance, transport error between point correspondences) and $\epsilon_s[\eta]$ is the Schwarzian penalizer:

$$\epsilon_s = \lambda \int_{\Omega} \left(S_1[\eta]^2 + S_2[\eta]^2 + S_3[\eta]^2 + S_4[\eta]^2 \right) d_{\Omega}, \tag{24}$$

where λ is a hyperparameter which weighs the influence of the Schwarzian derivatives over the data term. In practice we replace the integral in equation (24) with a sum over a discretization $\widetilde{\Omega}$ of the domain Ω:

$$\epsilon_s \approx \lambda \sum_{\mathbf{p}_i \in \widetilde{\Omega}} \sum_{k=1}^{4} S_k[\eta](\mathbf{p}_i)^2. \tag{25}$$

The Schwarzian penalty is quartic and non-convex. Solving the optimization problem (23) thus requires iterative optimization. We use the Levenberg-Marquardt algorithm.

5 Experimental Results

We compare Schwarp to state of the art warps, namely the BS-warp [24], TPS-warp [6], DP-warp [5] and NURBS-warp [7]. In table 1 we summarize the details of warps used in our experiments.

Table 1. Summary of warps used in our Experiments

Name	Warp Model	Penalizer
BS-warp	BS	Bending Energy
Schwarp	BS	Schwarzian Equations
TPS-warp	TPS	Bending Energy
DP-warp	DP	3D Bending Energy
NURBS-warp	NURBS	3D Bending Energy

5.1 Implementation Details

For the experiments with synthetic data, we generate a set of 100 images for each case while varying imaging conditions (pose and focal length) and present the average values for each of the criteria over the 100 images. We keep the resolution of the images at 640×480 pixels. We vary the focal length between 100 and 500 pixels. We fix the number of feature correspondences, control centers and a gaussian noise distribution (we vary the amount of noise for the same distribution). For all the other warps we use code publicly available from their authors.

5.2 Synthetic Data

We simulate images of rigid and deformable surfaces. In the rigid case, we use a plane and in the deformable case we wrap a surface around a longitudinal cut of a barrel. For both types of data, we examine the performance of all the warps against an increasing amount of noise, perspective and their sensitivity to the weight of the penalty. For the experiments with deformable surfaces, we add an additional experiment to compare them against an increasing amount of deformation. For all cases, we compare the warps based on three criteria: generalization error (ϵ_1), 1st derivative error (ϵ_2) and second derivative error (ϵ_3) compared to the ground truth. The generalization error is the transfer error measured in terms of RMSR (Root Mean Square Residual) between the warp and ground truth. This is computed over some points which were not used to estimate the warps. We give a relative error for the 1st and 2nd derivatives compared to ground truth.

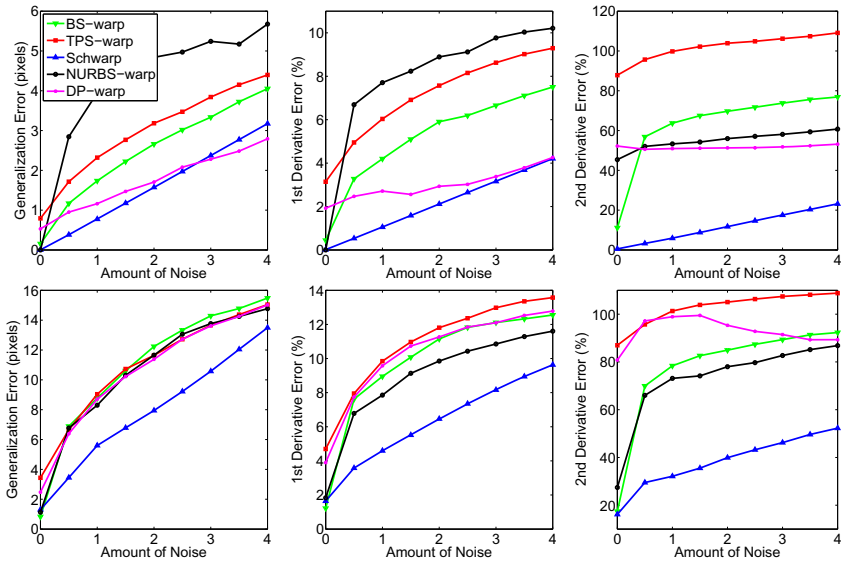

Fig. 3. Comparison of Schwarp with other warps against noise on synthetically generated images. The first and second rows are for the planar and deformable surfaces respectively.

Effect of Noise and Hyperparameter. We compute the warps with an increasing amount of noise and optimize the hyperparameter controlling smoothness in each case. Figure 3 presents the performance of all the warps against noise. In these experiments, Schwarp outperforms all the other warps in all criteria examined. This is true for both planar and deformable surfaces. As expected, the most significant improvement of Schwarp is in the case of 2nd derivatives. Schwarp does not penalize the bending energy and thus preserves the 2nd derivatives much better than any other warp that penalizes the bending energy.

To measure the sensitivities of the warps against the hyperparameter, we recompute all the warps as in the previous experiment. However, this time we do not optimize the hyperparameter in each case. Instead, we use the mean of the optimal hyperparameter of an image for all different noise level. This gives us 5 curves as in figure 3 but with larger errors since the hyperparameter is suboptimal for each case. For a given warp, the area between this new curve and the corresponding one in Figure 3 gives an estimate on a warp's sensitivity to the its hyperparameter. If this area is large, the warp is very sensitive to the hyperparameter. In table 2, we present the area between the two curves (with optimal and average hyperparameter) for all warps for planar and deformable case. It is clear from these results that Schwarp is the most stable against hyperparameter. In all cases, it undergoes the smallest deviation from the optimal curve.

Effect of Perspective. We compare the warps with a set of images with increasing perspective. To control the amount of perspective, we follow a single

Table 2. Sensitivities of the warps to their hyperparameter. The larger the number the more sensitive the warp to its hyperparameter.

Algorithms	Planar Case			Deformable Case		
	ϵ_1	ϵ_2	ϵ_3	ϵ_1	ϵ_2	ϵ_3
BS-warp	2.3948	0.0566	0.4630	10.2054	0.1172	0.4537
Schwarp	**0.0275**	**0.0006**	**0.0025**	**3.6637**	**0.0329**	**0.1098**
TPS-warp	2.0912	0.0470	0.1830	9.5280	0.0791	0.1895
DP-warp	10.1772	0.3194	1.2826	47.7706	0.1858	0.3079
NURBS-warp	0.4227	0.0216	0.3859	5.7904	0.1151	0.7170

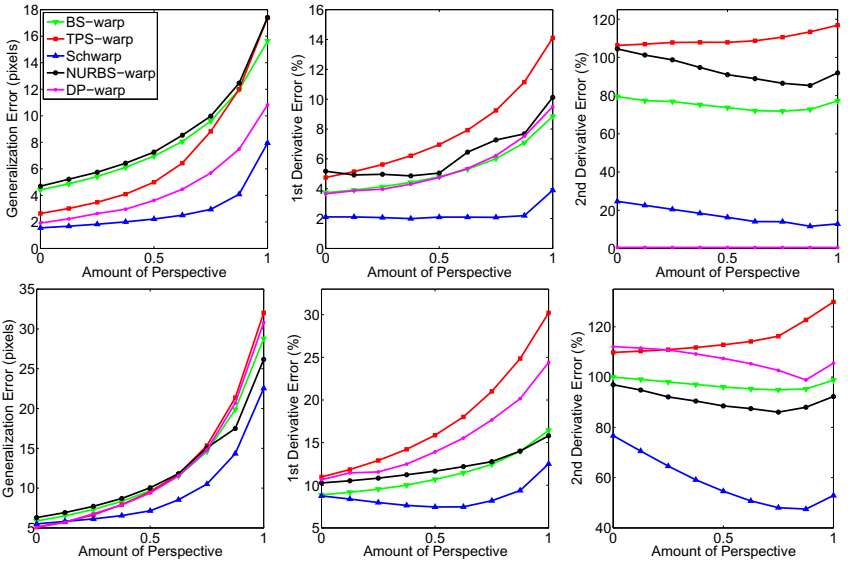

Fig. 4. Performance of the different warps against increasing amount of perspective. The first and second rows are for planar and deformable surfaces respectively.

parameter projection model that allows us to select the amount of perspective required. With this model, a point $P = [P_x, P_y, P_z]^\top$ is projected as:

$$\Pi_t(P) = \left((t+1) f \frac{P_x}{P_z + tf} \qquad (t+1) f \frac{P_y}{P_z + tf} \right)^\top . \tag{26}$$

Equation (26) becomes orthographic projection when $t \to \infty$. Figure 4 shows that Schwarp outperforms all the other warps with a significant margin. The errors increase linearly first, and then quadratically, with increasing perspective. It is interesting to note that Schwarp models perspective better than the rational warps (DP-warp and NURBS-warp).

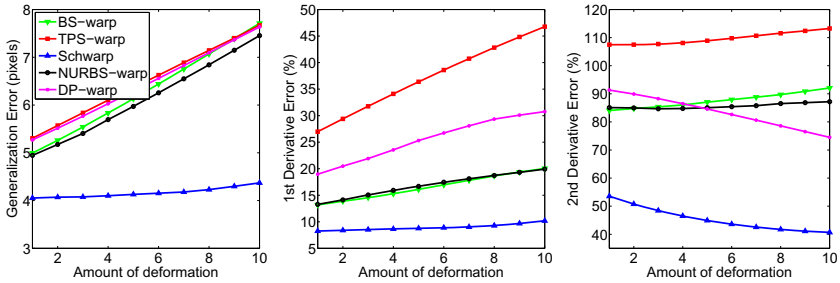

Fig. 5. Performance of different warps against increasing amount of deformation

(a) Shape 1 (b) Shape 2 (c) Shape 3 (d) Shape 4 (e) Shape 5 (f) Shape 6 (g) Shape 7

Fig. 6. Dataset used in the real experiments

Effect of Deformation. We examine the behavior of the warps with an increasing amount of deformation (figure 5). Deformation is controlled by changing different parameters of a curved surface. We can see a similar trend in this case: Schwarp performs better than all the other warps. The generalization error and the 1st and 2nd derivatives error degrade linearly with increasing deformation.

Rate of Convergence. In all experiments, we kept track of the number of iterations required for the non-linear refinement part of Schwarp, DP-warp and NURBS-warp to converge to a solution. Indeed these 3 warps use Levenberg-Marquardt for estimation. We have found that on an average Schwarp takes only 10-15 iterations to converge, whereas DP-warp and NURBS-warp require hundreds of iterations. This indicates that Schwarp is more stable numerically. This is due to the rational modeling of DP-warp and NURBS-warp.

5.3 Real Data

We compare the performance of the warps in different applications on real images. In Figure 6, we present the dataset used in the experiments. As a surface, we use a textured paper of size $210mm \times 297mm$. We deform the paper on several occasions and capture images of those deformations. The resolutions of these images are 3264×4928 pixels. The focal length used is 2534 pixels. For each deformation, we obtain the ground truth shape Ψ using Structure-from-Motion.

SfT. Here, we show the experimental results for SfT. In SfT, the shape of an image is inferred from the warp computed between a template and the image

Table 3. Reconstruction error (in mm) for SfT on the 7 images of Figure 6

	Shape 1	Shape 2	Shape 3	Shape 4	Shape 5	Shape 6	Shape 7
BS-warp	7.02	33.78	13.67	8.14	5.88	**10.42**	8.52
Schwarp	**3.24**	**30.02**	**10.49**	**8.08**	**2.06**	11.72	**7.99**
TPS-warp	21.08	46.20	18.81	10.41	17.19	15.46	11.88
DP-warp	16.95	43.74	14.05	10.26	6.82	13.62	11.28
NURBS-warp	8.38	45.69	15.56	10.10	6.70	15.78	12.46

Table 4. Relative calibration recovery error on the 7 images of Figure 6

	Shape 1	Shape 2	Shape 3	Shape 4	Shape 5	Shape 6	Shape 7
BS-warp	0.0247	0.0826	0.0475	**0.0267**	**0.0137**	0.0463	0.0063
Schwarp	**0.0071**	**0.0038**	0.0284	0.0275	**0.0137**	**0.0165**	**0.0055**
TPS-warp	0.0945	0.1793	0.0565	0.1287	0.2038	0.0712	0.0300
DP-warp	0.0577	0.1455	**0.0165**	0.1014	0.0512	0.0724	0.0263
NURBS-warp	0.0239	0.0985	0.0186	0.0798	0.0210	0.0561	0.0275

itself. In our implementation, we use a feature based approach to SfT. We use feature matching to find correspondences between the template and the target image and use those matches to compute the warp. Table 3 shows the reconstruction errors of SfT for each warp. The reconstruction error is computed between the reconstructed shape Ψ' and Ψ, using $\sum_{i,j\in\widetilde{\Omega}} |\Psi'_{i,j} - \Psi_{i,j})|$, where $\widetilde{\Omega}$ is the discretization of the domain. The errors are given in millimeters. In most cases, Schwarp outperforms the other warps. However, in one case, it gives the second best score after BS-warp.

Calibration in SfT. Calibration in SfT allows one to compute the focal length of the camera from the warp. We implemented the method proposed in [4]. We use all the computed warps for all the real images to recover the focal length($\hat{f}$). We compute the relative error from the true focal length f, using $\frac{|\hat{f}-f|}{f}$. The results are presented in Table 4. Here, our warp performs better than the other warps in 5 out of 7 cases.

6 Conclusion

In this paper, we have studied differential projective invariants and their application for modeling the projection of deforming surfaces. We have presented the 2D Schwarzian derivatives and we introduced a new type of penalty based on penalizing Schwarzian derivatives of the warp. Schwarzian derivatives model projective functions differentially. We have conducted experiments on real and simulated data. We have shown that Schwarps (Schwarzian penalized warps) notably improve accuracy in deformable surface reconstruction and camera calibration in SfT.

Acknowledgments. This research has received funding from the EU's FP7 ERC research grant 307483 FLEXABLE.

References

1. Astrom, K.: Fundamental limitations on projective invariants of planar curves. IEEE Transactions on Pattern Analysis and Machine Intelligence 17(1), 77–81 (1995)
2. Bartoli, A., Gérard, Y., Chadebecq, F., Collins, T.: On template-based reconstruction from a single view: Analytical solutions and proofs of well-posedness for developable, isometric and conformal surfaces. In: Computer Vision and Pattern Recognition (2012)
3. Bartoli, A., Zisserman, A.: Direct estimation of non-rigid registrations. In: British Machine Vision Conference (2004)
4. Bartoli, A., Collins, T.: Template-based isometric deformable 3D reconstruction with sampling-based focal length self-calibration. In: Computer Vision and Pattern Recognition (2013)
5. Bartoli, A., Perriollat, M., Chambon, S.: Generalized thin-plate spline warps. International Journal of Computer Vision 88(1), 85–110 (2010)
6. Bookstein, F.L.: Principal warps: Thin-plate splines and the decomposition of deformations. IEEE Transaction on Pattern Analysis Machine Intelligence 11(6), 567–585 (1989)
7. Brunet, F., Bartoli, A., Navab, N., Malgouyres, R.: NURBS warps. In: British Machine Vision Conference (2009)
8. Cayley, A.: On the Schwarzian derivatives and the polyhedral functions. Transaction of Cambridge Philosophical Society 13 (1880)
9. Faugeras, O.D., Luong, Q.T., Papadopoulo, T.: The Geometry of Multiple Images: The Laws that Govern the Formation of Multiple Images of a Scene and Some of Their Applications. MIT Press (2001)
10. Hartley, R.I., Zisserman, A.: Multiple View Geometry in Computer Vision. Cambridge University Press (2003) ISBN: 0521623049
11. Horn, B., Schunck, B.: Determining optical flow. Artificial Intelligence 17, 185–203 (1981)
12. Kummer, E.E.: Über die hypergeometrische reihe. Journal Fur Die Reine Und Angewandte Mathematik 1836(15), 39–83 (1836)
13. Lazebnik, S., Ponce, J.: The local projective shape of smooth surfaces and their outlines. International Journal of Computer Vision 63, 65–83 (2005)
14. Lei, G.: Recognition of planar objects in 3D space from single perspective views using cross ratio. IEEE Transactions on Robotics and Automation 6(4), 432–437 (1990)
15. Matsumoto, K., Sasaki, T., Yoshida, M.: Recent progress of gauss-schwartz theory and related geometric structures. Memoirs of the Faculty of Science 47(2), 283–381 (1993)
16. Molzon, R., Mortensen, K.P.: The Schwarzian derivative for maps between manifolds with complex projective connections. Transactions of the American Mathematical Society 348(8), 3015–3036 (1996)
17. Mundy, J.L., Zisserman, A.: Geometric invariance in computer vision. MIT Press (1992)

18. Oda, T.: On schwarzian derivatives in several variables. Kokyuroku Research Institute for Mathematical Sciences 226, 82–85 (1974) (in Japanese)
19. Osgood, B., Stowe, D.: The Schwarzian derivative and conformal mapping of Riemannian manifolds. Duke Mathematical Journal 67(1), 57–99 (1992)
20. Ovsienko, V.: Lagrange Schwarzian derivative. Moscow University Mechanics Bulletin 44(6), 8–13 (1989)
21. Ovsienko, V., Tabachnikov, S.: Projective Differential Geometry Old and New: From the Schwarzian Derivative to the Cohomology of Diffeomorphism Groups. Cambridge University Press (2005)
22. Ovsienko, V., Tabachnikov, S.: What is...the Schwarzian derivative? North American Mathematical Society 56, 34–36 (2009)
23. Pilet, J., Lepetit, V., Fua, P.: Fast non-rigid surface detection, registration and realistic augmentation. International Journal of Computer Vision 76(2), 109–122 (2007)
24. Rueckert, D., Sonoda, L.I., Hayes, C., Hill, D.L.G., Leach, M.O., Hawkes, D.J.: Nonrigid registration using free-form deformations: Application to breast MR images. IEEE Transactions on Medical Imaging 18, 712–721 (1999)
25. Salzmann, M., Pilet, J., Ilic, S., Fua, P.: Surface deformation models for nonrigid 3D shape recovery. Transactions on Pattern Analysis and Machine Intelligence 29(8), 1481–1487 (2007)
26. Schmid, C., Zisserman, A.: The geometry and matching of lines and curves over multiple views. International Journal of Computer Vision 40, 199–233 (2000)
27. Singer, D.: Stable orbits and bifurcation of maps of the interval. SIAM Journal of Applied Mathematics 35(2), 260–267 (1978)
28. Szeliski, R.: Image alignment and stitching: A tutorial. Foundations and Trends in Computer Graphics and Computer Vision 2(1), 1–104 (2006)
29. Torr, P.: MLESAC: A new robust estimator with application to estimating image geometry. Computer Vision and Image Understanding 78, 138–156 (2000)
30. Torresani, L., Hertzmann, A., Bregler, C.: Non-rigid structure-from-motion: Estimating shape and motion with hierarchical priors. IEEE Transactions on Pattern Analysis and Machine Intelligence 30(5), 878–892 (2008)